Computer Assisted Mechanics and Engineering Sciences, 10: 479–494, 2003.

Hybrid Finite Element – Wave Based Method for acoustic problems

Bas van Hal, Wim Desmet, Dirk Vandepitte, Paul Sas
Katholieke Universiteit Leuven
Department of Mechanical Engineering, Division PMA
Celestijnenlaan 300B
B-3001, Heverlee, Belgium

(Received September 11, 2003)

The finite element method (FEM) is widely accepted for the steady-state dynamic response analysis of acoustic systems. It exhibits almost no restrictions with respect to the geometrical features of these systems. However, its application is practically limited to the low-frequency range. An alternative method is the wave based method, which is an indirect Trefftz method. It exhibits better convergence properties than the FEM and therefore allows accurate predictions at higher frequencies. However, the applicability is limited to systems of moderate geometrical complexity.

The coupling between both methods is proposed. Only the parts of the problem domain with a complex geometry are modelled using the FEM, while the remaining parts are described with a wave based model. The proposed hybrid method has the potential to cover the mid-frequency range, where it is still difficult for currently existing (deterministic) techniques to provide satisfactory prediction results within a reasonable computational time.

1. Introduction

The Helmholtz equation governs the steady-state acoustic pressure fields in cavities. The finite element method (FEM) is widely used for the analysis of such acoustic problems [1, 2]. The numerical procedure consists of subdividing an acoustic cavity in a large number of small subdomains, i.e. the finite elements. The FEM exhibits almost no restrictions with respect to the geometrical features of the considered problem domain, because the subdivision in finite elements is possible for arbitrarily shaped systems. Within each element, a linear combination of simple (polynomial) basis functions approximates the field variables. The basis functions do not satisfy the governing Helmholtz equation. Consequently, the FEM cannot approximate efficiently the spatial variation of the dynamic field variables for higher frequencies due to the involved interpolation errors and dispersion errors [2]. The dispersion errors result from the difference between the numerical wavenumber and the physical wavenumber of the problem and they become the dominant sources of error at higher frequencies. The number of elements and the subsequent computational efforts have to increase drastically for increasing frequency to keep the approximation errors within reasonable limits. This restricts the practical use of the FEM to low-frequency applications.

Alternative deterministic methods are desired, which suffer less from dispersion errors in order to allow accurate predictions at higher frequencies. The broad family of Trefftz methods satisfies this requirement [3–6]. These methods apply approximation functions, which satisfy a priori the governing differential equations.

Various applications of the Trefftz method to the Helmholtz equation have been reported in literature, a.o. [7–17]. This paper considers the wave based method (WBM) [16, 17]. The WBM is an indirect Trefftz method, based on the application of wave-type functions. The numerical procedure consists of subdividing the cavity in large (convex) subdomains. The wave based (WB)

approximation functions satisfy the Helmholtz equation, but they violate the boundary conditions and the interface conditions. Either a weighted residual formulation or a least-squares formulation enforces the WB approximation to satisfy these conditions in an integral sense.

The WBM exhibits better convergence properties than the FEM. The computational efficiency is most pronounced for acoustic systems, which can be subdivided in a small number of subdomains with a regular shape. The computational efficiency decreases, if the number of subdomains grows for reasons of system geometrical complexity. The application of the WBM is therefore limited to systems of moderate geometrical complexity.

In order to exploit the advantageous features of both methods, i.e. the wide application range of the FEM and the high convergence rate of the WBM, the coupling between both prediction tools is proposed [18, 19]. The basic idea is to replace those parts in the finite element (FE) mesh, that have a simple geometrical shape, by much smaller WB models. The resulting hybrid model has less degrees of freedom (DOF's) and a smaller computational load. This allows a further model refinement, which leads to an improved accuracy at higher frequencies. Figure 1 illustrates this procedure for a 2-dimensional (2D) car cavity. The proposed hybrid finite element – wave based (FE-WB) method has the potential to cover the so-called mid-frequency range, in which it is difficult for the currently existing (deterministic) techniques to provide accurate prediction results within a reasonable computational time.

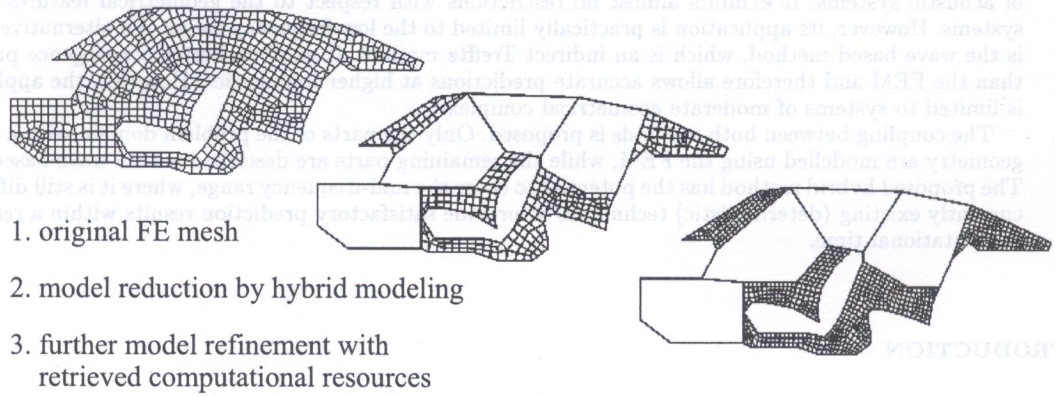

Fig. 1. Coupled FE-WB approach for 2D car cavity

The paper is arranged as follows. After the introduction of the mathematical description of the class of 2D bounded acoustic problems, the theoretical background of the FEM and the WBM are reviewed. The steady-state dynamic analysis of a simple acoustic system demonstrates the better convergence properties of the WBM compared to the FEM. The next part considers the derivation of the hybrid model. This part also covers the motivation for the selection of certain modelling principles. Finally, a simple example of a hybrid FE-WB model shows the computational potentials of the hybrid method.

2. Review of numerical prediction methods

2.1. Acoustic problem definition

Consider a 3D homogeneous acoustic cavity, of which the dimension in the z-direction is infinite. If both the dynamic loads and the boundary conditions do not vary in the z-direction, then the 3D problem can be reduced to a 2D problem, as depicted in Fig. 2.

The bounded acoustic problem consists of the acoustic cavity Ω surrounded by the boundary Γ. The boundary Γ is composed of three parts ($\Gamma = \Gamma_p \cup \Gamma_v \cup \Gamma_Z$), namely the boundary Γ_p with a prescribed pressure $\overline{p}$, the boundary Γ_v with a prescribed normal velocity $\overline{v}_n$ and the boundary Γ_Z

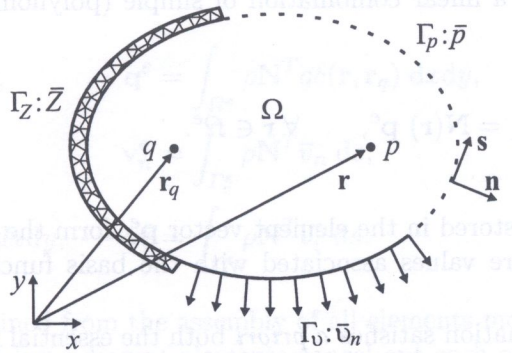

Fig. 2. 2D interior acoustic problem

with a prescribed normal impedance $\overline{Z}$. Furthermore, an acoustic line source q at position $\mathbf{r}_q$ excites the cavity Ω. The following inhomogeneous Helmholtz equation governs the steady-state pressure p at position $\mathbf{r}$

$$\left(\Delta + k^2\right)\, p = -j\rho\omega q\delta(\mathbf{r}, \mathbf{r}_q), \text{ in } \Omega, \tag{1}$$

together with the boundary conditions

$$\begin{cases} p &= \overline{p}, & \text{at } \Gamma_p \\ \mathcal{L}_v(p) &= \overline{v}_n, & \text{at } \Gamma_v \\ \mathcal{L}_v(p) &= p/\overline{Z}, & \text{at } \Gamma_Z \end{cases} \qquad \text{with } \mathcal{L}_v = \frac{j}{\rho\omega}\frac{\partial}{\partial n}. \tag{2}$$

$\Delta = \partial^2/\partial x^2 + \partial^2/\partial y^2$ represents the Laplace operator, $k = \omega/c$ the wavenumber with the speed of sound c, $j = \sqrt{-1}$ the unit imaginary number, ρ the ambient fluid density, ω the radial excitation frequency and δ the Dirac delta function. The linear operator $\mathcal{L}_v$ in Eq. (2), applied to the pressure, results in the velocity in the outward normal direction $\mathbf{n}$.

2.2. FEM applied to bounded acoustic problems

The acoustic cavity Ω is subdivided in a large number of elements resulting in an FE mesh, as shown in Fig. 3. Each element Ω^e is surrounded by the element boundary Γ^e, which is composed of four parts ($\Gamma^e = \Gamma^e_p \cup \Gamma^e_v \cup \Gamma^e_Z \cup \Gamma^e_i$). These parts are the intersections of the element boundary and the problem boundary ($\Gamma^e_p = \Gamma^e \cap \Gamma_p$, $\Gamma^e_v = \Gamma^e \cap \Gamma_v$ and $\Gamma^e_Z = \Gamma^e \cap \Gamma_Z$) and the common interface Γ^e_i between two adjacent elements.

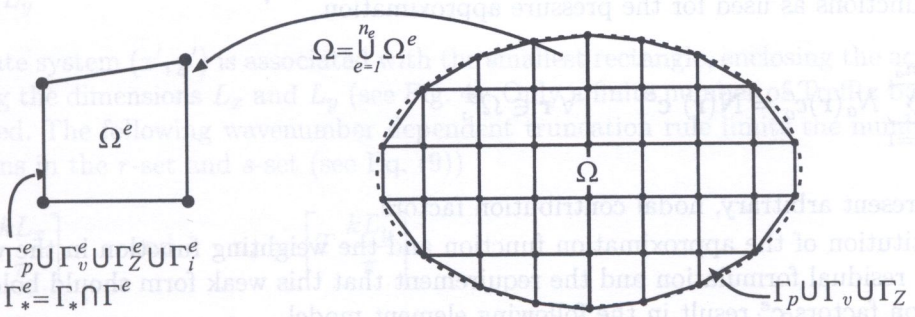

Fig. 3. FE subdivision and element definition

Within each element Ω^e, a linear combination of simple (polynomial) basis functions approximates the exact solution

$$p(\mathbf{r}) \approx \hat{p}(\mathbf{r}) = \sum_{a=1}^{n_a} N_a(\mathbf{r}) p_a^e = \mathbf{N}(\mathbf{r})\ \mathbf{p}^e, \qquad \forall\, \mathbf{r} \in \Omega^e. \tag{3}$$

The contribution factors p_a^e, stored in the element vector $\mathbf{p}^e$, form the unknown DOF's. In general, the DOF's are nodal pressure values associated with the basis functions N_a, stored in the row vector $\mathbf{N}$.

Assume that the approximation satisfies *a priori* both the essential boundary conditions and the inter-element pressure continuity for two adjacent elements (conforming elements). The approximation violates the Helmholtz Eq. (1) and the mixed and natural boundary conditions in Eq. (2). The introduced errors are forced to zero in an integral sense. Furthermore, the velocity continuity at the interface Γ_i^e between two adjacent elements has to be enforced. This results in the following weighted residual formulation for one element

$$\begin{aligned} &\int_{\Omega^e} W\left(\Delta\hat{p} + k^2\hat{p} + j\rho\omega q\delta(\mathbf{r},\mathbf{r}_q)\right) \mathrm{d}x\mathrm{d}y + \int_{\Gamma_v^e} j\rho\omega W\left(\mathcal{L}_v(\hat{p}) - \overline{v}_n\right) \mathrm{d}s + \ldots \\ &\quad \ldots + \int_{\Gamma_Z^e} j\rho\omega W\left(\mathcal{L}_v(\hat{p}) - \hat{p}/\overline{Z}\right) \mathrm{d}s + \int_{\Gamma_i^e} j\rho\omega W\left(\mathcal{L}_v(\hat{p}) - v_i^e\right) \mathrm{d}s = 0, \end{aligned} \tag{4}$$

where W represents a weighting function, s the tangential coordinate on the element boundary and v_i^e the unknown interface velocity. Some parts of the element boundary $\Gamma^e (= \Gamma_p^e \cup \Gamma_v^e \cup \Gamma_Z^e \cup \Gamma_i^e)$ may be empty, such that the corresponding integrals in Eq. (4) may vanish.

The approximation function $\hat{p}$ and the weighting function W in the weighted residual formulation must be C_1 continuous and C_{-1} continuous, respectively. By application of partial integration and the divergence theorem [20], the weighted residual formulation is transformed into its weak form

$$\begin{aligned} &\int_{\Omega^e} \left(-(\boldsymbol{\nabla} W)^T(\boldsymbol{\nabla}\hat{p}) + k^2 W\hat{p} + j\rho\omega W q\delta(\mathbf{r},\mathbf{r}_q)\right) \mathrm{d}x\mathrm{d}y + \ldots \\ &\quad \ldots - \int_{\Gamma_v^e} j\rho\omega W\overline{v}_n \mathrm{d}s - \int_{\Gamma_Z^e} j\rho\omega W\hat{p}/\overline{Z}\mathrm{d}s - \int_{\Gamma_i^e} j\rho\omega W v_i^e \mathrm{d}s = 0, \end{aligned} \tag{5}$$

where ^{T} denotes the transpose and where $\boldsymbol{\nabla} = [\partial/\partial x\ \partial/\partial y]^T$ represents the gradient operator. The continuity requirement of the approximation function $\hat{p}$ reduces to C_0 continuity, while the weighting function W has to be C_0 continuous too. Furthermore, the assumption is made that the weighting function W is zero on the parts of the boundary where essential boundary conditions are imposed. Following the Galerkin approach, the weighting function is chosen to be a linear combination of the same basis functions as used for the pressure approximation

$$W(\mathbf{r}) = \sum_{a=1}^{n_a} N_a(\mathbf{r}) c_a^e = \mathbf{N}(\mathbf{r})\ \mathbf{c}^e, \qquad \forall\, \mathbf{r} \in \Omega^e, \tag{6}$$

where c_a^e represent arbitrary, nodal contribution factors.

The substitution of the approximation function and the weighting function in the weak form of the weighted residual formulation and the requirement that this weak form should hold for any set of contribution factors $\mathbf{c}^e$ result in the following element model

$$\left(-\omega^2\mathbf{M}^e + j\omega\mathbf{C}^e + \mathbf{K}^e\right)\mathbf{p}^e = j\omega(\mathbf{q}^e - \mathbf{v}_n^e - \mathbf{v}_i^e), \tag{7}$$

with

$$\mathbf{M}^e = \int_{\Omega^e} c^{-2}\mathbf{N}^T\mathbf{N}\,\mathrm{d}x\mathrm{d}y, \qquad \mathbf{q}^e = \int_{\Omega^e} \rho\mathbf{N}^T q\delta(\mathbf{r},\mathbf{r}_q)\,\mathrm{d}x\mathrm{d}y,$$
$$\mathbf{C}^e = \int_{\Gamma_Z^e} (\rho/\overline{Z})\mathbf{N}^T\mathbf{N}\,\mathrm{d}s, \qquad \mathbf{v}_n^e = \int_{\Gamma_v^e} \rho\mathbf{N}^T\overline{v}_n\,\mathrm{d}s,$$
$$\mathbf{K}^e = \int_{\Omega^e} (\boldsymbol{\nabla}\mathbf{N})^T(\boldsymbol{\nabla}\mathbf{N})\,\mathrm{d}x\mathrm{d}y, \qquad \mathbf{v}_i^e = \int_{\Gamma_i^e} \rho\mathbf{N}^T v_i^e\,\mathrm{d}s.$$

The global FE model is obtained from the assembly of all elements models. In this assembly procedure, the contributions $\mathbf{v}_i^e$ of two adjacent elements cancel out each other. The essential boundary conditions are taken into account by assigning the prescribed pressure values directly to the nodal DOF's on the problem boundary Γ_p, such that these DOF's are no longer unknown. The reader is referred to references [1] and [2] for more details on the derivation of the FE model.

2.3. WBM applied to bounded acoustic problems

The WBM uses an approximation function, which is globally defined, i.e. on the entire problem domain, instead of on element level. It satisfies the inhomogeneous Helmholtz equation, but it violates the boundary conditions. The pressure field approximation is a linear combination of Trefftz basis functions, extended with a particular solution function $\hat{p}_q$

$$\hat{p} = \hat{p}(\mathbf{r}) = \sum_{a=1}^{n_a} \Phi_a(\mathbf{r})p_a + \hat{p}_q(\mathbf{r}) = \boldsymbol{\Phi}(\mathbf{r})\ \mathbf{p} + \hat{p}_q(\mathbf{r}), \qquad \forall\,\mathbf{r}\in\Omega. \tag{8}$$

The row vector $\boldsymbol{\Phi}$ contains Trefftz basis functions Φ_a, that satisfy the homogeneous Helmholtz equation. The unknown contribution factors p_a, stored in the column vector $\mathbf{p}$, form the unknown DOF's of the WB model. The DOF's do not represent nodal pressure values as in the case of the FEM. The method is named after the set of Trefftz basis functions, which consists of propagating and evanescent wave functions, defined as

$$\Phi_a(\mathbf{r}) = \begin{cases} \Phi_r(x',y') &= \cos(k_{rx}x')\mathrm{e}^{-jk_{ry}y'}, \\ \Phi_s(x',y') &= \mathrm{e}^{-jk_{sx}x'}\cos(k_{sy}y'), \end{cases} \tag{9}$$

with

$$\begin{cases} k_{rx} = \dfrac{r\pi}{L_x} & \text{and} \quad k_{ry} = \pm\sqrt{k^2 - k_{rx}^2}, \quad \text{for } r = 0,1,\ldots,n_r, \\ k_{sy} = \dfrac{s\pi}{L_y} & \text{and} \quad k_{sx} = \pm\sqrt{k^2 - k_{sy}^2}, \quad \text{for } s = 0,1,\ldots,n_s. \end{cases}$$

The coordinate system (x',y') is associated with the smallest rectangle, enclosing the acoustic cavity Ω and having the dimensions L_x and L_y (see Fig. 4). Only a finite number of Trefftz basis functions can be applied. The following wavenumber dependent truncation rule limits the number of Trefftz basis functions in the r-set and s-set (see Eq. (9))

$$n_r = \left\lceil T\frac{kL_x}{\pi}\right\rfloor \qquad \text{and} \qquad n_s = \left\lceil T\frac{kL_y}{\pi}\right\rfloor, \tag{10}$$

where $\lceil\ \rfloor$ represents the round operator to the nearest integer towards infinity and T a user defined truncation parameter. The truncation rule implies that the smallest wavelength of the cosine functions in the Trefftz basis functions is T times smaller than the acoustic wavelength $\lambda = 2\pi/k$.

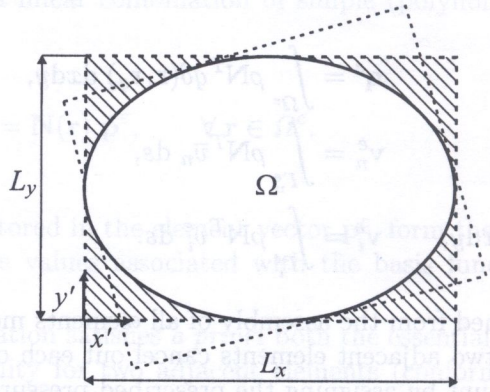

Fig. 4. (Smallest) enclosing rectangle for cavity Ω

The particular solution function $\hat{p}_q$ in Eq. (8) is associated with the cylindrical acoustic source q in the cavity Ω

$$\hat{p}_q(\mathbf{r}) = \frac{1}{4}\,\rho\omega\, q\, H_0^{(2)}\left(k\|\mathbf{r}-\mathbf{r}_q\|\right), \tag{11}$$

where $H_0^{(2)}$ is the zero-order Hankel function of the second kind.

The wave approximation $\hat{p}$ violates the acoustic boundary conditions in Eq. (2). Either a weighted residual formulation or a least-squares formulation enforces the approximation to satisfy these conditions in an integral sense. In [18] and [19], the least-squares formulation has been discussed. Here, the following weighted residual formulation is used

$$-\int_{\Gamma_p} \mathcal{L}_v(W)(\hat{p}-\overline{p})\mathrm{d}s + \int_{\Gamma_v} W\left(\mathcal{L}_v(\hat{p})-\overline{v}_n\right)\mathrm{d}s + \int_{\Gamma_Z} W\left(\mathcal{L}_v(\hat{p})-\hat{p}/\overline{Z}\right)\mathrm{d}s = 0, \tag{12}$$

where W represents a weighting function.

Following the Galerkin approach, the weighting function is chosen to be a linear combination of the same Trefftz basis functions as used for the pressure approximation

$$W(\mathbf{r}) = \sum_{a=1}^{n_a} \Phi_a(\mathbf{r}) c_a = \mathbf{\Phi}(\mathbf{r})\,\mathbf{c}, \qquad \forall\, \mathbf{r} \in \Omega, \tag{13}$$

where c_a represent arbitrary contribution factors.

The substitution of the pressure approximation and the weighting function in the weighted residual formulation and the requirement that this formulation should hold for any set of contribution factors $\mathbf{c}$ result in the following WB model

$$\left(\mathbf{A}_p + \mathbf{A}_v + \mathbf{A}_Z\right)\mathbf{p} = \mathbf{b}_p + \mathbf{b}_v + \mathbf{b}_Z, \tag{14}$$

with

$$\mathbf{A}_p = -\int_{\Gamma_p} \mathcal{L}_v\left(\mathbf{\Phi}^T\right)\mathbf{\Phi}\,\mathrm{d}s, \qquad \mathbf{b}_p = -\int_{\Gamma_p} \mathcal{L}_v\left(\mathbf{\Phi}^T\right)\left(\overline{p}-\hat{p}_q\right)\mathrm{d}s,$$

$$\mathbf{A}_v = \int_{\Gamma_v} \mathbf{\Phi}^T \mathcal{L}_v\left(\mathbf{\Phi}\right)\mathrm{d}s, \qquad \mathbf{b}_v = \int_{\Gamma_v} \mathbf{\Phi}^T\left(\overline{v}_n - \mathcal{L}_v\left(\hat{p}_q\right)\right)\mathrm{d}s,$$

$$\mathbf{A}_Z = \int_{\Gamma_Z} \mathbf{\Phi}^T\left(\mathcal{L}_v\left(\mathbf{\Phi}\right) - \mathbf{\Phi}/\overline{Z}\right)\mathrm{d}s, \qquad \mathbf{b}_Z = -\int_{\Gamma_Z} \mathbf{\Phi}^T\left(\mathcal{L}_v\left(\hat{p}_q\right) - \hat{p}_q/\overline{Z}\right)\mathrm{d}s.$$

Since the contribution factors of the Trefftz basis functions are the unknown DOF's, which are not nodal values of the field variables, the pressure approximation in each point of the cavity Ω is computed in a post-processing step using Eq. (8).

The reader is referred to references [16] and [17] for more details on the WBM.

2.4. FEM-WBM comparison

First, the features of FE models and WB models are compared. An FE model consists of large but sparse, symmetric model matrices. The model matrices are composed of frequency independent submatrices. A WB model consists of symmetric matrices that are small compared to FE model matrices. The model matrices are, however, fully populated and not composed of frequency independent submatrices.

The FEM requires a large number of elements to keep the approximation errors within reasonable limits. If the approximation errors are kept constant, then the FE model size has to grow with frequency. This would require the construction of many FE meshes, which is practically impossible. Therefore, in general, one FE mesh is constructed, for which the approximation errors at the highest frequency of interest are acceptable. Consequently, this strategy does not make optimal use of the computational resources in the sense that the FE model is "too accurate" if a broad frequency spectrum is considered. The WBM requires a new WB model for each frequency, because the model matrices are not composed of frequency independent submatrices. This strategy allows one to practically keep the approximation errors constant over the total frequency range.

Next, the convergence behaviour of both methods are compared for a simple numerical example. Consider the simple 2D acoustic system, shown in Fig. 5. It consists of a bounded acoustic domain filled with air ($\rho = 1.225$ kg/m^3, $c = 340$ m/s), which represents a simplified car cavity. A prescribed velocity of $\overline{v}_n = 1$ m/s of the fire wall at $x = 0$ m excites the acoustic system. A prescribed normal impedance of $\overline{Z} = \rho c$ at the ceiling introduces some damping.

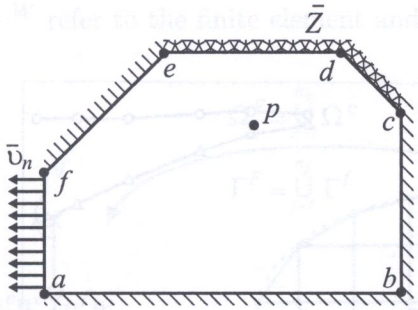

ID	x in m	y in m
a	0.00	0.00
b	1.50	0.00
c	1.50	0.75
d	1.25	1.00
e	0.50	1.00
f	0.00	0.50
p	0.88	0.70

Fig. 5. 2D simplified 2D car cavity

Figure 6 shows the response spectra of the pressure at a discrete cavity position obtained with three different numerical models. An FE model consists of linear quadrilateral elements and contains 725 DOF's. A WB model uses a truncation parameter of $T = 2$. A third model serves as reference model and consists of a very accurate FE model of approximately 5000 DOF's, which is constructed using quadratic quadrilateral elements. The comparison of the three spectra shows that the WBM does not suffer from dispersion errors. The resonance peaks of WBM results coincide with the reference results, even in the upper part of the considered frequency range. On the other hand, the resonance peaks of the FEM results coincide only with the reference results at low frequencies (approximately below 600 Hz).

The convergence behaviour of both methods is considered at two distinct frequencies, one in the low frequency range (350 Hz) and one in the mid-frequency range (1700 Hz). Both frequencies are indicated with vertical cursor lines in Fig. 6. Figure 7 shows the corresponding convergence curves. The plotted relative pressure error is defined as

$$\left\| \frac{\hat{p} - p_{\text{ref}}}{p_{\text{ref}}} \right\|, \tag{15}$$

where $\hat{p}$ represents either the FE or WB pressure approximation at the considered response point and where p_{ref} is the pressure at the response point obtained with the reference model. Clearly,

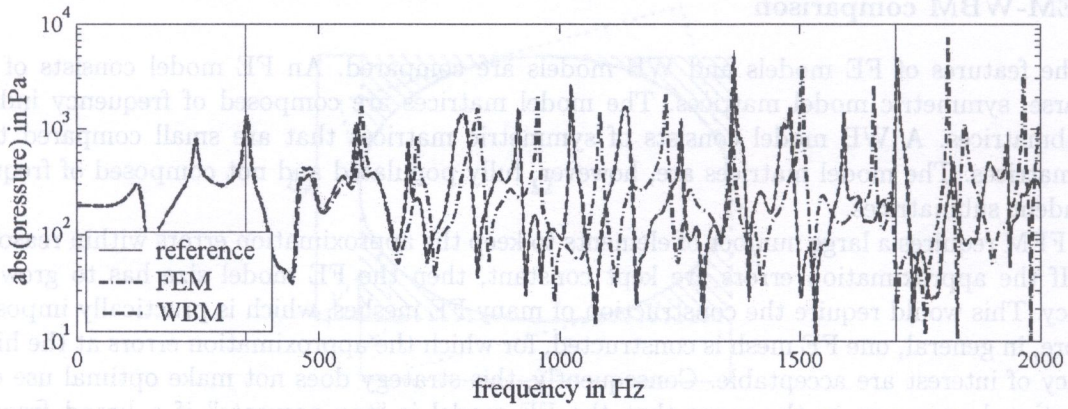

Fig. 6. Pressure response spectrum

the WBM exhibits better convergence properties. The overall WBM error level is below the overall FEM error level with substantially smaller model sizes. Furthermore, the slope of the convergence curves is higher for the WBM. The WBM has the potential to produce accurate approximations also in the mid-frequency range, as is illustrated by the curves associated with the frequency of 1700 Hz. At this frequency, the FEM is still not converging, even with a fine FE of approximately 4000 DOF's.

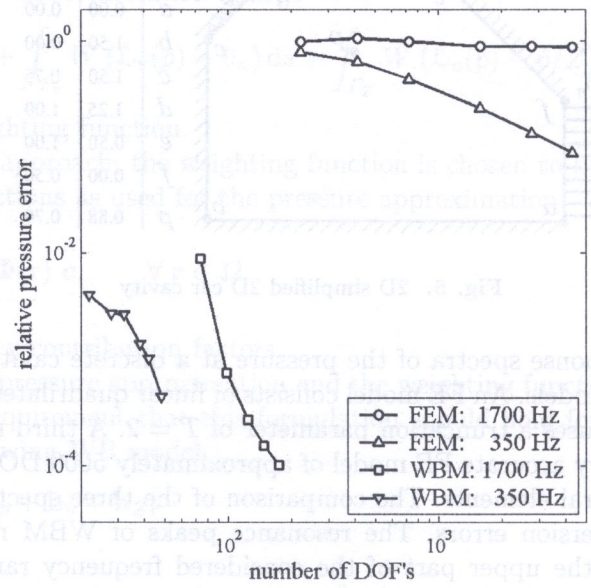

Fig. 7. Convergence curves

The numerical example, presented here, shows that the WBM exhibits better convergence properties than the FEM in that less DOF's are required to obtain good accuracy. Various validations [16, 17, 21] have shown that the smaller model sizes result also in significant reduction of the computational time. A sufficient condition to achieve this enhanced convergence is that the considered cavity is convex. Otherwise, a domain decomposition strategy can be employed, however, at the expense of some loss in computational efficiency [16, 17]. The computational benefits of the WBM can therefore only be exploited for systems of moderate geometrical complexity.

3. Hybrid Finite Element – Wave Based Method

3.1. Introduction

The coupling between the FEM and the WBM is proposed to exploit the advantageous features of both methods, i.e. the geometrical flexibility of the FEM and the high convergence rate of the WBM. Fig. 1 illustrates the basic idea of this approach. Small WB models replace those parts of the FE subdivision, which have a simple geometrical shape. The resulting hybrid model contains less DOF's. The subsequent computational resources that are saved, compared to the original FE model, allow a further model refinement, so that this strategy may lead to an improved accuracy at higher frequencies.

3.2. Hybrid FE-WB method applied to bounded acoustic problems

Consider the division of an acoustic cavity as shown in Fig. 8. The subdomain Ω^E is modelled by the FEM and the subdomain Ω^W by the WBM. Each subdomain is surrounded by a part of the boundary $\Gamma^\bullet = \Gamma_p^\bullet \cup \Gamma_v^\bullet \cup \Gamma_Z^\bullet$ and by the FE-WB interface Γ^F. The following interface conditions hold at Γ^F

$$\begin{aligned} p^e &= p^W \qquad \text{(pressure continuity)}, \\ \mathcal{L}_v^e(p^e) &= -\mathcal{L}_v^W(p^W) \quad \text{(velocity continuity)}, \end{aligned} \tag{16}$$

where superscripts ^{e} and ^{W} refer to the finite element and the wave model, respectively.

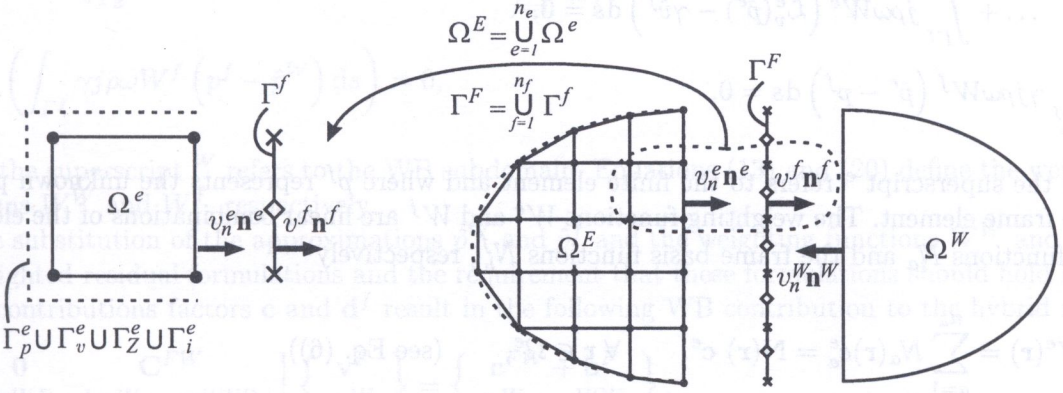

Fig. 8. Coupled FE-WB approach

In the hybrid approach, the interface conditions are satisfied in an integral sense by the application of the Lagrange multiplier technique (LMT) [1]. The procedure consists of placing a fictitious frame at the FE-WB interface Γ^F on which the Lagrange multiplier is defined. Here, a velocity frame is applied with the frame velocity v^f as Lagrange multiplier. The velocity frame is subdivided in n_f line elements ($\Gamma^F = \cup_{f=1}^{n_f} \Gamma^f$), that are matching geometrically the edges of the finite element subdomain Ω^e. Within each line element, a linear combination of simple (polynomial) basis functions approximates the frame velocity v^f as follows

$$v^f(s) \approx \hat{v}^f(s) = \sum_{b=1}^{n_b} N_b^f(s) v_b^f = \mathbf{N}^f(s)\mathbf{v}^f, \qquad \forall\, s \in \Gamma^f. \tag{17}$$

The contribution factors v_b^f, stored in the column vector $\mathbf{v}^f$, are additional unknown DOF's associated with the frame basis functions N_b^f, stored in the row vector $\mathbf{N}^f$. The approximation $\hat{v}^f$ is

discontinuous at the interface vertices by the application of basis functions N_b^f, which belong for example to the family of 1D hierarchical functions based on mid-side nodes [1, 5, 6].

The frame velocity forms an additional natural boundary condition for each subdomain

$$\begin{aligned} v_n^e &= \gamma v^f \\ v_n^W &= -\gamma v^f \end{aligned} \quad \text{at } \Gamma^f \text{ with } \gamma = \mathbf{n}^{e\,T}\mathbf{n}^f = -\mathbf{n}^{W\,T}\mathbf{n}^f, \tag{18}$$

where $\mathbf{n}^e$, $\mathbf{n}^f$ and $\mathbf{n}^W$ represent the outward normal vectors of the finite element Ω^e, of the frame element Γ^f and of the WB submodel, respectively.

First, the construction of the FE part of the hybrid FE-WB model is considered. The FE element model is obtained by enforcing the FEM approximation errors on the following relations to zero in an integral sense: (i) the Helmholtz equation in Ω^e, (ii) the boundary conditions at Γ_v^e and Γ_Z^e, (iii) the inter-element velocity continuity at the interface Γ_i^e between two adjacent elements and (iv) the velocity continuity at the interface Γ^f. According to the LMT, the pressure continuity at the interface Γ^f is considered separately in order to obtain additional equations to account for the additional frame DOF's. The following weighted residual formulations are applied, similar to the FE formulation considered in Section 2.2

$$\begin{aligned} &\int_{\Omega^e} W^e \left(\Delta\hat{p}^e + k^2\hat{p}^e + j\rho\omega q\delta(\mathbf{r},\mathbf{r}_q)\right) \mathrm{d}x\mathrm{d}y + \int_{\Gamma_v^e} j\rho\omega W^e \left(\mathcal{L}_v^e(\hat{p}^e) - \overline{v}_n\right) \mathrm{d}s + \ldots \\ &\quad \ldots + \int_{\Gamma_Z^e} j\rho\omega W^e \left(\mathcal{L}_v^e(\hat{p}^e) - \hat{p}^e/\overline{Z}\right) \mathrm{d}s + \int_{\Gamma_i^e} j\rho\omega W^e \left(\mathcal{L}_v^e(\hat{p}^e) - v_i^e\right) \mathrm{d}s + \ldots \\ &\quad \ldots + \int_{\Gamma^f} j\rho\omega W^e \left(\mathcal{L}_v^e(\hat{p}^e) - \gamma\hat{v}^f\right) \mathrm{d}s = 0, \\ &\int_{\Gamma_i^f} \gamma j\rho\omega W^f \left(\hat{p}^e - p^f\right) \mathrm{d}s = 0, \end{aligned} \tag{19}$$

where the superscript ^{e} refers to the finite element and where p^f represents the unknown pressure at the frame element. The weighting functions W^e and W^f are linear combinations of the elemental basis functions N_a and the frame basis functions N_b^f, respectively

$$\begin{aligned} W^e(\mathbf{r}) &= \sum_{a=1}^{n_a} N_a(\mathbf{r}) c_a^e = \mathbf{N}(\mathbf{r})\ \mathbf{c}^e, \qquad \forall\, \mathbf{r} \in \Omega^e, \qquad \text{(see Eq. (6))}, \\ W^f(s) &= \sum_{b=1}^{n_b} N_b^f(s) d_b^f = \mathbf{N}^f(s)\ \mathbf{d}^f, \qquad \forall\, s \in \Gamma^f. \end{aligned} \tag{20}$$

where c_a^e and d_b^f represent arbitrary contribution factors.

The FE element model is derived from the presented weighted residual formulation by a two-step procedure. First, the application of partial integration and the divergence theorem on the first relation in Eq. (19) relaxes the continuity requirements for the element pressure approximation $\hat{p}^e$ (see Section 2.2). The first weighted residual formulation in Eq. (19) is transformed into its weak form. Then, the substitution of the approximations $\hat{p}^e$ and $\hat{v}^f$ and the weighting functions W^e and W^f in the obtained weighted residual formulations and the requirement that these formulations should hold for any set of contributions factors $\mathbf{c}^e$ and $\mathbf{d}^f$ result in the following element contribution to the hybrid model

$$\begin{bmatrix} \mathbf{Z}^e & \mathbf{C}^{ef} \\ \mathbf{C}^{fe} & \mathbf{0}, \end{bmatrix} \begin{Bmatrix} \mathbf{p}^e \\ \mathbf{v}^f \end{Bmatrix} = \begin{Bmatrix} \mathbf{f}^E \\ \mathbf{b}^f \end{Bmatrix} \quad \text{with} \quad \begin{cases} \mathbf{Z}^e = -\omega^2\mathbf{M}^e + j\omega\mathbf{C}^e + \mathbf{K}^e, \\ \mathbf{f}^e = j\omega(\mathbf{q}^e - \mathbf{v}_n^e - \mathbf{v}_i^e). \end{cases} \tag{21}$$

$\mathbf{M}^e$, $\mathbf{C}^e$, $\mathbf{K}^e$, $\mathbf{q}^e$, $\mathbf{v}_n^e$ and $\mathbf{v}_i^e$ represent the uncoupled FE submodel contributions as defined in Eq. (7). $\mathbf{C}^{ef}$ represents the elemental FE – frame coupling matrix defined as

$$\mathbf{C}^{ef} = j\omega \int_{\Gamma f} \gamma\rho \mathbf{N}^T \mathbf{N}^f \, \mathrm{d}s = \mathbf{C}^{fe\,T} \tag{22}$$

and the vector $\mathbf{b}^f$ is defined as

$$\mathbf{b}^f = -j\omega \int_{\Gamma f} \gamma\rho \mathbf{N}^{f\,T} p^f \, \mathrm{d}s. \tag{23}$$

The global FE submodel is obtained by a straightforward assembly process, in which the contributions $\mathbf{v}_i^e$ of two adjacent elements cancel out each other. The contributions $\mathbf{b}^f$ will vanish at the time the FE submodel is coupled to the WB submodel.

Next, the construction of the WB part of the hybrid FE-WB model is considered. The WB model contribution is obtained by enforcing the WBM approximation errors on the following relations to zero in an integral sense: (i) the boundary conditions at Γ_p^W, Γ_v^W and Γ_Z^W and (ii) the velocity continuity at the interface Γ^F. Again, according to the LMT, the pressure continuity at the interface Γ^F is considered separately in order to obtain additional equations to account for the additional frame DOF's. The following weighted residual formulations are applied, similar to the WBM considered in Section 2.3

$$\begin{aligned} &-\int_{\Gamma_p} \mathcal{L}_v(W^W)(\hat{p}^W - \overline{p}) \, \mathrm{d}s + \int_{\Gamma_v} W^W \left(\mathcal{L}_v^W(\hat{p}^W) - \overline{v}_n\right) \mathrm{d}s + \ldots \\ &\ldots + \int_{\Gamma_Z} W^W \left(\mathcal{L}_v^W(\hat{p}^W) - \hat{p}^W/\overline{Z}\right) \mathrm{d}s + \bigcup_{f=1}^{n_f} \left(\int_{\Gamma f} W^W \left(\mathcal{L}_v(\hat{p}^W) + \gamma \hat{v}^f \right) \mathrm{d}s \right) = 0, \\ &\bigcup_{f=1}^{n_f} \left(\int_{\Gamma f} \gamma j\rho\omega W^f \left(p^f - \hat{p}^W \right) \mathrm{d}s \right) = 0, \end{aligned} \tag{24}$$

where the superscript ^{W} refers to the WB subdomain. Equations (13) and (20) define the weighting functions W^W and W^f, respectively.

The substitution of the approximations $\hat{p}^W$ and $\hat{v}^f$ and the weighting functions W^W and W^f in the weighted residual formulations and the requirement that these formulations should hold for any set of contributions factors $\mathbf{c}$ and $\mathbf{d}^f$ result in the following WB contribution to the hybrid model

$$\begin{bmatrix} \mathbf{0} & \mathbf{C}^{FW} \\ \mathbf{C}^{WF} & (\mathbf{A}^W + \mathbf{C}^{WW}) \end{bmatrix} \begin{Bmatrix} \mathbf{v}^F \\ \mathbf{p}^W \end{Bmatrix} = \begin{Bmatrix} \mathbf{c}^{FW} + \mathbf{b}^F \\ \mathbf{b}^W + \mathbf{c}^{WW} \end{Bmatrix}, \tag{25}$$

where $\mathbf{v}^F$ collects all the unknown frame DOF's $\mathbf{v}^f$. $\mathbf{A}^W$ and $\mathbf{b}^W$ represent the uncoupled WB model contributions as defined in Eq. (14). $\mathbf{C}^{WW}$ and $\mathbf{c}^{WW}$ represent the WB model back-coupling matrix and WB model back-coupling vector, respectively, defined as

$$\begin{aligned} \mathbf{C}^{WW} &= \bigcup_{f=1}^{n_f} \left(\int_{\Gamma f} \mathbf{\Phi}^T \mathcal{L}_v^W(\mathbf{\Phi}) \, \mathrm{d}s \right), \\ \mathbf{c}^{WW} &= -\bigcup_{f=1}^{n_f} \left(\int_{\Gamma f} \mathbf{\Phi}^T \mathcal{L}_v^W(\hat{p}_q) \, \mathrm{d}s \right). \end{aligned} \tag{26}$$

$\mathbf{C}^{WF}$ represents the WB model – frame coupling matrix defined as

$$\mathbf{C}^{WF} = \bigcup_{f=1}^{n_f} \left(\int_{\Gamma f} \gamma \mathbf{\Phi}^T \mathbf{N}^f \, \mathrm{d}s \right). \tag{27}$$

$\mathbf{C}^{FW}$ and $\mathbf{c}^{FW}$ represent the frame – WB model coupling matrix and the frame – WB model coupling vector, respectively, defined as

$$\begin{aligned} \mathbf{C}^{FW} &= -j\omega \bigcup_{f=1}^{n_f} \left(\int_{\Gamma^f} \gamma\rho \mathbf{N}^{f^T} \mathbf{\Phi} \, \mathrm{d}s \right), \\ \mathbf{c}^{FW} &= \; j\omega \bigcup_{f=1}^{n_f} \left(\int_{\Gamma^f} \gamma\rho \mathbf{N}^{f^T} \hat{p}_q \, \mathrm{d}s \right). \end{aligned} \tag{28}$$

The vector $\mathbf{b}^F$ is defined as

$$\mathbf{b}^F = j\omega \bigcup_{f=1}^{n_f} \left(\int_{\Gamma^f} \gamma\rho \mathbf{N}^{f^T} p^f \mathrm{d}s \right). \tag{29}$$

The final hybrid FE-WB model follows from the assembly of the submodels in Eqs. (21) and (25)

$$\begin{bmatrix} \mathbf{Z}^E & \mathbf{C}^{EF} & \mathbf{O} \\ \mathbf{C}^{FE} & \mathbf{O} & \mathbf{C}^{FW} \\ \mathbf{O} & \mathbf{C}^{WF} & (\mathbf{A}^W + \mathbf{C}^{WW}) \end{bmatrix} \begin{Bmatrix} \mathbf{p}^E \\ \mathbf{v}^F \\ \mathbf{p}^W \end{Bmatrix} = \begin{Bmatrix} \mathbf{f}^E \\ \mathbf{c}^{FW} \\ \mathbf{b}^W + \mathbf{c}^{WW} \end{Bmatrix}, \tag{30}$$

where $\mathbf{p}^E$ collects all the FE DOF's. The contributions $\mathbf{b}^f$ and $\mathbf{b}^F$ cancel out each other at the interface between the FE submodel and the WB submodel.

The system matrix of the hybrid model in Eq. (30) contains both large sparse submatrices and small dense submatrices. In order to apply suited solution strategies for both types of submatrices, the FE DOF's can be eliminated from the hybrid model as follows

$$\begin{bmatrix} -\mathbf{C}^{FE} \left(\mathbf{Z}^E\right)^{-1} \mathbf{C}^{EF} & \mathbf{C}^{FW} \\ \mathbf{C}^{WF} & (\mathbf{A}^W + \mathbf{C}^{WW}) \end{bmatrix} \begin{Bmatrix} \mathbf{v}^F \\ \mathbf{p}^W \end{Bmatrix} = \begin{Bmatrix} \mathbf{c}^{FW} - \mathbf{C}^{FE} \left(\mathbf{Z}^E\right)^{-1} \mathbf{f}^E \\ (\mathbf{b}^W + \mathbf{c}^{WW}) \end{Bmatrix}. \tag{31}$$

The above procedure benefits from the sparsity of the FE model, since the expressions $\left(\mathbf{Z}^E\right)^{-1} \mathbf{C}^{EF}$ and $\left(\mathbf{Z}^E\right)^{-1} \mathbf{f}^E$ can be computed with efficient solvers for sparse linear systems. The FE DOF's are recovered by the following matrix-vector multiplication using the solution of Eq. (31)

$$\mathbf{p}^E = \left(\mathbf{Z}^E\right)^{-1} \mathbf{f}^E - \left(\mathbf{Z}^E\right)^{-1} \mathbf{C}^{EF} \mathbf{v}^F, \tag{32}$$

where the expressions $\left(\mathbf{Z}^E\right)^{-1} \mathbf{C}^{EF}$ and $\left(\mathbf{Z}^E\right)^{-1} \mathbf{f}^E$ have already been computed in Eq. (31).

3.3. Numerical example

Consider the simple 2D acoustic problem, which has been discussed in Section 2.4. This problem is well suited to demonstrate the potentials of the hybrid FE-WB method. Starting point is the FE model shown in Fig. 9, which consists of linear quadrilateral element and contains 725 DOF's. The hybrid FE-WB model is derived from this FE model by replacing a large number of elements in the lower part of the acoustic cavity by a WB submodel with a truncation factor $T = 2$ (see Fig. 9). Again, the very accurate FE model, used in Section 2.4, serves as reference model. Table 1 lists the sizes of the three models. Recall that the size of the WB submodel is frequency dependent. The model sizes are therefore given for five discrete frequencies.

Figure 10 shows the response spectra of the pressure at the discrete cavity position obtained with the reference model, the FE model (FEM-1) and the hybrid FE-WB model (HM-1). The upper frequency limit is restricted to 1200 Hz, since the response spectrum, obtained with the FE

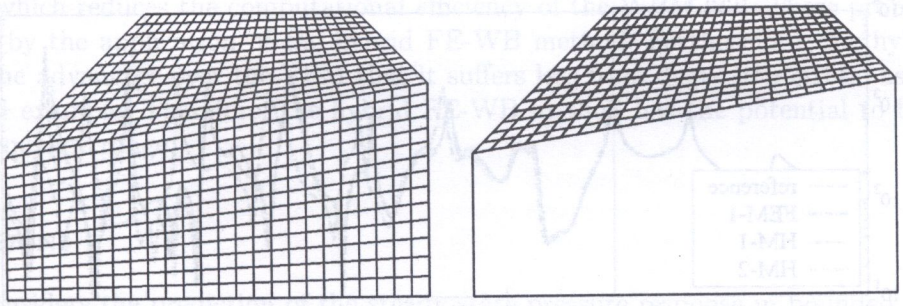

Fig. 9. FE model and hybrid FE-WB model (configuration 1)

Table 1. Model properties for FEM and hybrid FE-WB method comparison

model	frequency in Hz	number of DOF's			
		FE	frame	WB	total
reference†		4787			4787
FEM-1		725			725
HM-1	300	375	24	22	421
	450	"	"	28	427
	600	"	"	38	437
	750	"	"	46	445
	900	"	"	52	451
	1050	"	"	62	461
	1200	"	"	70	469
HM-2	300	316	51	30	397
	450	"	"	40	407
	600	"	"	50	417
	750	"	"	62	429
	900	"	"	70	437
	1050	"	"	82	449
	1200	"	"	90	457

† *constructed using quadratic quadrilateral elements*

model, suffers too much from dispersion errors. The plot shows clearly that the hybrid FE-WB model suffers less from dispersion errors than the FE model. The response spectrum of the hybrid FE-WB model coincides with reference solution below 800 Hz and the resonance peaks are predicted accurately even up to 1200 Hz.

The convergence behaviour of the hybrid FE-WB method is compared to convergence behaviour of the FEM and the WBM. The model refinement for the hybrid FE-WB method constists of a mesh refinement of the FE submodel only. The convergence analysis is considered at one distinct frequency in the low frequency range only (350 Hz), because the convergence analysis in Section 2.4 has shown that the FEM has not converged at 1700 Hz due to the large dispersion erros, even for large model sizes. Figure 11 shows the improved convergence behaviour of the hybrid FE-WB method (HM-1) with respect to the FEM (FEM-1).

Next, the influence of the subdivision of the acoustic cavity is considered briefly. A second FE mesh, shown in Fig. 12, provides a slightly different response prediction for the pressure with respect to the original FE mesh, shown in Fig. 9. The derived hybrid FE-WB model, which contains two WB subdomains (see Fig. 12), will therefore provide different pressure approximations than the original

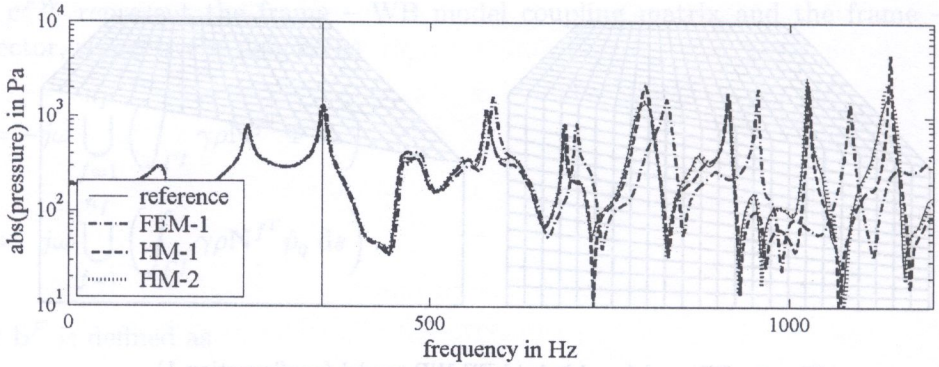

Fig. 10. Pressure response spectrum

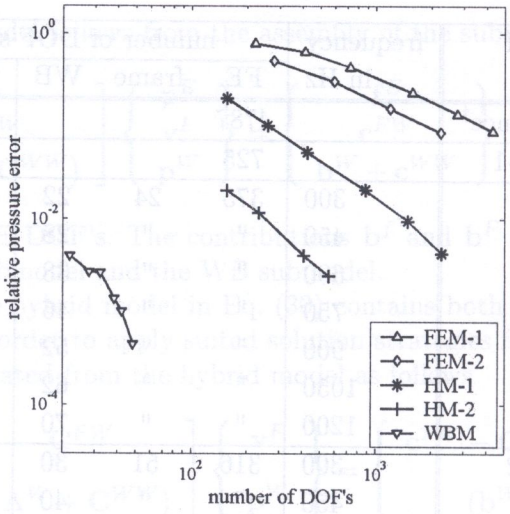

Fig. 11. Convergence curves

hybrid WB-FE model. Figure 10 shows that the response spectrum, obtained with this alternative hybrid FE-WB model (HM-2), is closer to the reference solution. Also, the convergence behaviour has been improved as shown by the HM-2 curve in Fig. 11. Future investigations will focus on the influence the domain subdivision on the prediction accuracy with the objective to obtain rules for optimal domain subdivision.

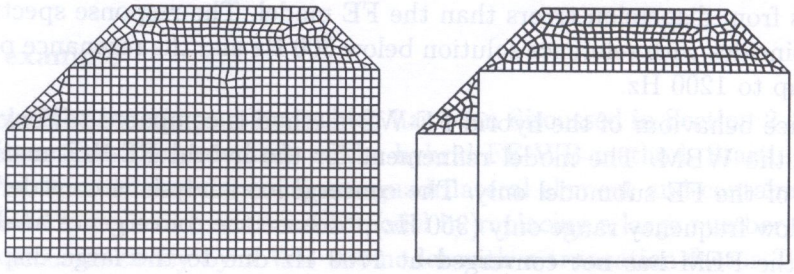

Fig. 12. FE model and hybrid FE-WB model (configuration 2)

Finally, this numerical example shows that still the WBM exhibits the best convergence properties. However, in practice, it is not always possible to subdivide an acoustic cavity in convex subdomains [19]. Furthermore, this domain decomposition strategy may involve a large number of

subdomains, which reduces the computational efficiency of the WBM [22]. These problems may be circumvented by the application of the hybrid FE-WB method. Furthermore, the hybrid FE-WB method has the advantage over the FEM that it suffers less from dispersion errors, as is shown by this numerical example. Therefore, the hybrid FE-WB method has the potential to be applicable in the mid-frequency range.

4. Conclusions

This paper considers the prediction of the steady-state pressure response in bounded acoustic systems. The FEM is well suited for this application, however it is restricted to the low-frequency range. A large number of elements is required to keep the approximation errors within reasonable limits. Especially, the dispersion errors cause problems for increasing frequencies.

There is a need for deterministic methods that suffer less from dispersion errors, such that these methods can be used for higher frequencies. The broad family of Trefftz methods satisfies this requirement. This paper considers one such method, namely the WBM. The WBM exhibits better convergence properties than the FEM. However, the computational efficiency decreases if domain decomposition is required to cope with systems of high geometrical complexity.

The coupling between the FEM and the WBM is proposed to exploit the advantageous features of both methods, i.e. the unrestricted geometrical complexity of FE models and the high convergence rate of the WBM. The idea is to reduce the overall computational efforts by replacing large parts of an FE model with a much smaller WB model. The paper presents the mathematical description of this hybrid modelling strategy.

It is illustrated through a validation example that the hybrid model can produce more accurate results than the FE model from which it is derived by replacing a large number of finite elements by a smaller WB model. The validation demonstrates the potentials of the hybrid FE-WB method, in that it exhibits an enhanced convergence rate with a reduced numerical dispersion, compared to a full FE approach. In this way, the hybrid approach may allow mid-frequency analyses within reasonable computational efforts.

Acknowledgments

The research of B. van Hal is financed by a scholarship of the Institute for the Promotion of Innovation by Science and Technology in Flanders (IWT).

References

[1] O. C. Zienkiewicz and R. L. Taylor. *The Finite Element Method – Volume 1: Basic formulation and linear problems.* McGraw-Hill, London, 4th edition, 1989.

[2] F. Ihlenburg. *Finite Element Analysis of Acoustic Scattering*, volume 132 of *Applied Mathematical Sciences.* Springer, New York, 1998.

[3] E. Trefftz. Ein Gegenstück zum Ritzschen Verfahren. In: *Proceedings of Second International Congress on Applied Mechanics*, pages 131–137, Zürich, 1926.

[4] E. Kita and N. Kamiya. Trefftz method: an overview. *Advances in Engineerging Software*, **24**: 3–12, 1995.

[5] J. Jirousek and A. Wroblewski. T-elements: state of the art and future trends. *Archives of Computational Mechanics in Engineering*, **3**: 323–434, 1996.

[6] Q.-H. Qin. *The Trefftz Finite and Boundary Element Method.* WIT Press, 2000.

[7] Y. K. Cheung, W. G. Jin, and O. C. Zienkiewicz. Solution of Helmholtz equation by Trefftz method. *International Journal for Numerical Methods in Engineering*, **32**: 63–78, 1991.

[8] I. Herrera. Trefftz–Herrera domain decomposition. *Advances in Engineering Software*, **24**: 43–56, 1995.

[9] S. C. Huang and R.P. Shaw. The Trefftz method as an integral equation. *Advances in Engineering Software*, **24**: 57–63, 1995.

[10] M. Stojek. Least-squares Trefftz-type elements for the Helmholtz equation. *International Journal for Numerical Methods in Engineering*, **41**: 831–849, 1998.

[11] P. Monk and D.-Q. Wang. A least-squares method for the Helmholtz equation. *Computer Methods in Applied Mechanics and Engineering*, **175**: 121–136, 1999.

[12] J. A. Teixeira de Freitas. Hybrid-Trefftz displacement and stress elements for elastodynamics analysis in the frequency domain. *Computer Assisted Mechanics and Engineering Sciences*, **4**: 345–368, 1997.

[13] Y. Y. Kim and J. H. Kang. Free vibration analysis of membranes using wave-type base functions. *Journal of the Acoustical Society of America*, **99**: 2938–2946, 1996.

[14] Y. Y. Kim and D. K. Kim. Applications of waveguide-type base functions for the eigenproblems of two-dimensional cavities. *Journal of the Acoustical Society of America*, **106**: 1704–1711, 1999.

[15] S. Lifits, S. Reutskiy, and B. Tirozzi. A new Trefftz method for solving boundary value problems. *ARI*, **50**: 85–95, 1997.

[16] W. Desmet. *A wave based prediction technique for coupled vibro-acoustic analysis.* PhD thesis, Katholieke Universiteit Leuven, 1998.

[17] W. Desmet, B. van Hal, P. Sas, and D. Vandepitte. A computationally efficient prediction technique for the steady-state dynamic analysis of coupled vibro-acoustic systems. *Advances in Engineering Software*, **33**: 527–540, 2002.

[18] B. van Hal, W. Desmet, D. Vandepitte, and P. Sas. A Coupled Finite Element – Wave Based Approach for the steady-state dynamic analysis of acoustic systems. In: R. Boone, editor, *Proceedings of Internoise 2001*, pages 2459–2464, NAG, The Hague, 2001.

[19] B. van Hal, W. Desmet, D. Vandepitte, and P. Sas. A Coupled Finite Element – Wave Based Approach for the steady-state dynamic analysis of coupled structural-acoustic systems. In: H. A. Mang, F. G. Rammerstorfer, and J. Eberhardsteiner, editors, *Proceedings of the Fifth World Congress on Computational Mechanics (WCCM V)*, Austria, 2002. Vienna University of Technology.

[20] M. D. Greenberg. *Advanced Engineering Mathematics.* Prentice Hall, Upper Saddle River, NJ, USA, 2nd edition, 1998.

[21] B. van Hal, A. Hepberger, H.-H. Priebsch, W. Desmet, and P. Sas. High perfomance implementation and conceptual development of the wave based method for the steady-state dynamic analysis of acoustic problems. In: P. Sas and B. van Hal, editors, *Proceedings of ISMA2002 – International Conference on Noise and Vibration Engineering*, pages 817–826, Leuven, 2002. Katholieke Universiteit Leuven.

[22] P. Sas, W. Desmet, B. van Hal, and B. Pluymers. On the use of a wave based prediction technique for vehicle interior acoustics. In: *Proceedings Styrian NVH Congress*, pages 175–185, Graz, 2001.